Multi-proxy reconstruction of surface water pCO_2 in the northern Arabian Sea since 29 ka

M.R. Palmer [a*], G.J. Brummer [b], M.J. Cooper [a], H. Elderfield [c], M.J. Greaves [c], G.J. Reichart [d], S. Schouten [b], J.M. Yu [e]

[a] *NOC, School of Ocean & Earth Science, University of Southampton, European Way, Southampton, SO14 3ZH, UK*

[b] *Royal Netherlands Institute of Sea Research NIOZ, Departments of Geology & Marine Organic Biogeochemistry, Den Burg, Texel NL-1790 AB Netherlands*

[c] *Department of Earth Sciences, University of Cambridge, Cambridge, CB3 3EQ, UK*

[d] *University of Utrecht, Faculty of Earth Sciences, Department of Geochemistry, Utrecht, NL-3508 TA Netherlands*

[e] *Columbia University, Lamont Doherty Earth Observatory, Palisades, NY 10964 USA*

* Corresponding author:

e-mail: pmrp@noc.soton.ac.uk tel: +44(0)2380596607

fax: +44(0)2380593059

Abstract

We report here the results of a multi-proxy study to reconstruct surface water pCO_2 concentrations in the northern Arabian Sea. Our results show that $\delta^{11}B$ and Mg/Ca measurements of the planktonic foraminifer *Globigerinoides sacculifer* yield consistent pCO_2 values with those reconstructed from the $\delta^{13}C$ of alkenones when used in

conjunction with foraminifera $\delta^{13}C$ and Cd/Ca values. They reveal that this area of the oceans has been a constant source of CO_2 to the atmosphere during the interval 5-29 ka, and that the intensity of this source was greatest between 11-17 ka, when atmospheric CO_2 levels were rising rapidly. We interpret our data as reflecting variation in the strength of the Asian summer monsoon (ASM), thus indicating that the strength of the ASM varied in phase with summer insolation over the Tibetan plateau between 5-29 ka. In contrast to a previous study (Clemens and Prell, 2003), we observe no significant lag between the rise in insolation and the response of the ASM. Rather, our data support a recent study by Rohling et al. (2009) that northern hemisphere climatic forcing factors play a greater role in controlling the intensity of the ASM during times of intense monsoon activity, and that the southern hemisphere forcing is more important during times of weak monsoons.

Key words: Arabian Sea; monsoon; carbon dioxide; palaeoceanography

1. Introduction

It is well known that atmospheric pCO_2 has varied over glacial-interglacial time scales (Indermühle et al., 1999; Smith et al., 1999), and there is general consensus that the oceans have played a major role in regulating these changes (e.g. Broecker, 1982). While there is considerable debate concerning the exact mechanisms by which the oceans act to change atmospheric pCO_2 (e.g. Archer and Maier-Reimer, 1994; Anderson et al., 2002), there must have been changes in the surface areas of the ocean that are supersaturated or undersaturated with CO_2 with respect to the atmosphere, or changes in the magnitude of the degree of supersaturation or undersaturation.

Thanks to many years of intensive oceanographic campaigns, we now have a good understanding of the present-day geographic distribution of the pCO_2 of ocean surface waters and the CO_2 fluxes between the ocean and atmosphere (Takahashi et al., 2002). Briefly, the Arabian Sea upwelling system is second only to the Eastern Equatorial Pacific as an oceanographic source of atmospheric CO_2, with the major oceanographic sinks occurring at latitudes of 35-55^{o}S and in the northern North Atlantic and Norwegian Sea (Takahashi et al., 2002). Clearly, if we were able to reconstruct maps of past variations in surface ocean pCO_2 we would be in a much better position to understand the causes of glacial-interglacial changes in atmospheric pCO_2. With this in mind, several proxies have been proposed for surface water pCO_2 and applied to various areas and time scales. The two proxies that have received the most attention are the boron isotope ($\delta^{11}B$) composition of planktonic foraminifera (Palmer and Pearson, 2003) and the carbon isotope ($\delta^{13}C_{alk}$) composition of alkenones (Pagani, 2002). Recently, it has been proposed that the B/Ca ratio of planktonic foraminifera might also serve as a

59 pCO_2 proxy (Yu et al., 2007; Foster, 2008). While these studies yield results that appear
60 to be consistent with other oceanographic and climatologic observations, there has yet to
61 be a study in which the efficacy of these proxies is compared at single site over the same
62 time interval.

63 Here, we report the results of a multi-proxy study ($\delta^{11}B$, B/Ca and $\delta^{13}C_{alk}$) of
64 surface water pCO_2 values in the northern Arabian Sea over the past 29 kyr. The basic
65 aspects of the monsoon system in the Arabian Sea are well understood (Wyrtki, 1973).
66 Strong monsoonal winds in the area lead to large seasonal changes in hydrography and
67 particle fluxes. At the most fundamental level the monsoon is controlled by changes in
68 atmospheric pressure over the Tibetan plateau. During the northern winter increases in
69 snow cover and cooling of the Tibetan plateau and Siberia leads to high atmospheric
70 pressures over Central Asia. This, in turn, leads to a pressure gradient between Central
71 Asia and the Inter Tropical Convergence Zone and drives the northeast winds of the
72 winter monsoon. During the northern summer, the lower albedo over the Tibetan plateau
73 causes the overlying air to heat up and rise. The resultant pressure gradient between
74 Central Asia and the winter high over the southern ocean generates the Asian Summer
75 Monsoon (ASM) that draws in winds towards the Tibetan plateau, leading to strong
76 upwelling off the coast of Oman and advection of these waters into the Arabian Sea.
77 Alongside this overall controlling mechanism, the strength of the ASM is also linked to
78 both large scale oceanographic (e.g. ENSO) and atmospheric (e.g. southern hemisphere
79 tropospheric flow) forcing functions that can lead to significant deviations from a simple
80 insolation-driven monsoon model (Rodwell, 1997; Schott and McCreary, 2001)

Biological production in the Arabian Sea is generally low during winter, but the nutrient- and CO_2-rich upwelling water results in maxima in biological productivity and surface water pCO_2 values in the northern Arabian Sea between July and September (Schulte and Müller, 2001; Sarma, 2003). This regular seasonal pattern is modulated by both short- (inter-annual) and long-term (orbital-scale) variations in the strength of the ASM (Wang et al., 2005). In addition, there is considerable spatial heterogeneity in productivity and particle fluxes, as a result of limited duration eddies and wind curl events (Honjo et al., 1999). Hence, any attempt to reconstruct past variations in surface seawater conditions of the Arabian Sea from proxies must acknowledge that our understanding of the present day spatial and temporal variations of these proxies is incomplete (Wang et al., 2005).

Nevertheless, paleoceanographic studies generally show that over the past ~250 kyr the strength of the ASM is dominated by precession cycles ~21-23 kyr, that reflect orbitally-driven variations in the strength of summer insolation over the Tibetan plateau (Reichart et al., 1997; Clemens and Prell, 2003; Yuan et al., 2004; Huybers, 2006). However, there is disagreement as to whether peaks in ASM intensity are directly in phase with maxima in summer insolation (Yuan et al., 2004) or whether the ASM maxima lag insolation curves by up to 8 kyr (Clemens and Prell, 2003).

This study seeks to apply a multi-proxy approach ($\delta^{11}B$, B/Ca, Mg/Ca, Cd/Ca) to addressing the coherence between the intensity of the ASM and the strength of summer insolation over the interval 5-29 ka.

2. Material and Methods

We have chosen a site in the northern Arabian Sea as this area is presently an important source of CO_2 from the oceans to the atmosphere (Takahashi et al., 2002). Our samples were taken from core NIOP464 collected from the southern flank of the Murray Ridge (22.15°N, 63.35°E; water depth 1470 m). Sediments from this core have been subject to detailed study, including bulk geochemical composition, foraminifer abundances, foraminifer stable isotopes, carbon-14 dating and organic geochemistry (Reichart et al., 1997; Schouten et al., 2000). Foraminifer data were determined at Southampton ($\delta^{11}B$) and Cambridge (B/Ca, Mg/Ca and Cd/Ca), and alkenone data were determined at NIOZ using methods described by Palmer et al. (1998), Palmer and Pearson (2003) for $\delta^{11}B$, Yu et al. (2005) for element/Ca ratios, and Schouten et al. (2000) for alkenones.

3. Results

The foraminifer and alkenone data are reported in Table 1, together with the average analytical uncertainties for each of the proxies.

The age model for sediments from the NIOP464 piston core reported by Reichart et al. (1998) was established by comparison of the *Neogloboquadrina dutertrei* $\delta^{18}O$ record with SPECMAP $\delta^{18}O$ chronology (Imbrie et al., 1984; Martinson et al., 1987). In this study we also used material from the trigger weight core, with cross calibration of the two cores undertaken by four independent properties (Fig. 1).

The relative abundance of the planktonic foraminifer *Globigerina bulloides* has long been used as an indicator of monsoon upwelling conditions (Prell and Curry, 1981). In contrast, foraminifer assemblages dominated by *Globigerinoides sacculifer* and *G.*

127 *ruber* have often been taken to be indicative of non-upwelling conditions (Cayre et al.,
128 1999). The dynamic and highly variable nature of the monsoon means that there are
129 considerable spatial and temporal variations in the response of individual foraminifer
130 species to upwelling (Peeters and Brummer, 2002). However, sediment trap studies
131 during 1986-87 showed that seasonal variations in the absolute abundances of *G.*
132 *bulloides*, *G. sacculifer* and *G. ruber* in the Arabian Sea are similar (Curry et al., 1992).
133 The numbers of *G. sacculifer* and *G. ruber* specimens counted in the traps are typically 2
134 orders of magnitude lower than those of *G. bulloides* (Curry et al., 1992), so there is
135 considerably more variance in their distribution patterns. Nevertheless, all three species
136 show broadly coincident maxima during periods of upwelling (Fig. 2a). Hence, while the
137 relative abundances of *G. sacculifer* and *G. ruber* in the sedimentary record are lower
138 during upwelling periods (Ivanova et al., 2003) (because their numbers are diluted by the
139 faster growing *G. bulloides*) they carry proxy signals that are dominated by upwelling
140 conditions.

141 Studies of living *G. bulloides* and *G. sacculifer* off the Oman coast show that their
142 depth distributions overlap at both upwelling and non-upwelling sites, although it is
143 interesting to note that *G. bulloides* occurs at slightly shallower depths than *G. sacculifer*
144 in upwelling locations, whereas the opposite is true at non-upwelling sites (Peeters and
145 Brummer, 2002).

146 Hence, the *G. sacculifer* proxy signals likely show an understated response to
147 upwelling conditions relative to *G. bulloides*. While it might be desirable to study pH
148 variations recorded by the $\delta^{11}B$ of *G. bulloides*, unlike *G. sacculifer* this species has not
149 been calibrated against this proxy in core top or culture experiments. Overall, we believe

that patterns illustrated in Figure 2 (which were derived from a sediment trap close to the core location), together with the depth distributions of living *G. sacculifer*, suggest that the proxy signals measured in this species will be dominated by variations in the intensity of the monsoon.

The C_{37-39} alkenones are biomarkers of prymnesiophyte origin, largely derived from the coccolithophorids *Emiliania huxleyi* and *Gephyrocapsa oceanica* (Brassell, 1993). Analyses of sediment trap material collected during 1994-95 from the Arabian Sea show maxima coincident with the winter and summer monsoons, with the integrated alkenone flux derived from the summer monsoon being approximately four times greater than that from the winter monsoon (Prahl et al., 2000) (Fig. 2b). Unfortunately, there were no coincident measurements of foraminifer assemblages and alkenone fluxes from these two sediment trap studies. However, bulk $CaCO_3$ fluxes from the 1994-5 study (Prahl et al., 2000) show similar trends to the alkenone fluxes (Fig. 2b), and visual inspection of the sediment trap material suggests that foraminifers contribute significantly to the total $CaCO_3$ flux and may indeed dominate this contribution (Prahl et al., 2000).

Hence, while we concur with Wang et al. (2005) that our understanding of the spatial and temporal distribution of alkenones and the foraminifer species considered here is incomplete, the balance of the evidence suggests that the bulk of alkenones, *G. sacculifer* and *G. ruber* recovered from sediments in the northern Arabian Sea will have formed in the surface waters during summer monsoon periods.

Several studies have shown that the magnitude of the summer monsoon varies on millennial, centennial and decadal timescales in response to solar activity and other global climatic drivers, such as Heinrich events (Agnihotri et al., 2002; Herzschuh, 2006),

173 the El Nino Southern Oscillation (Abram et al., 2007) and the Atlantic Multi-decadal
174 Oscillation (Lu et al., 2006). As it was not always possible to measure all of the proxies
175 in the same sub sample of core material, we have presented the proxy data as 3 point
176 running means to smooth these short term variations.

177 Sea surface temperatures (SST) were reconstructed from the alkenone $U^{k'}_{37}$-index
178 (Brassell et al., 1986) and Mg/Ca ratios of *G. sacculifer* (Anand et al., 2003) (Fig. 3).
179 The close agreement between these independent proxies provides further support to the
180 coincidence of maxima in alkenone, *G. sacculifer* and *G. ruber* fluxes from the surface
181 ocean during the ASM (Sarma, 2003; Curry et al., 1992).

182 The pH values derived from the $\delta^{11}B$ values (Fig. 4a) utilize the empirical pH-
183 $\delta^{11}B$ relationship derived from culture experiments of *G. sacculifer* at different pH values
184 that also account for the potential role of algal symbionts associated with this species
185 (Sanyal et al., 2001). The temperature dependence of boron isotope fractionation also has
186 to be taken into account (using the formulation of Zeebe and Wolf-Gladrow (2001) and
187 the Mg/Ca data). In addition, a comparison study between $\delta^{11}B$ values measured at
188 Lamont Doherty (i.e. in the Sanyal et al. (2001) study) and at Southampton revealed a
189 consistent 2.2‰ offset between the two laboratories (Hönisch et al., 2003; Palmer and
190 Pearson, 2003). Both this study and that of Sanyal et al. (2001) employed negative ion
191 thermal ionization mass spectrometry (N-TIMS) to measure the boron isotope
192 compositions of the foraminifers. This method yields $\delta^{11}B$ values that are consistently
193 higher at equivalent pH values than those measured by multi-collector inductively
194 coupled mass spectrometry (MC-ICP-MS) (Foster, 2008), with the latter being more
195 consistent with the most recent experimental determination of the boron isotope

196 fractionation factor between $B(OH)_3$ and $B(OH)_4^-$ (Klochko et al., 2006). However,
197 several laboratories have demonstrated that the empirically calibrated N-TIMS technique
198 does yield calculated pH values for recent foraminifer that are consistent with present day
199 pH values in surface seawater (Palmer and Pearson, 2003; Hönisch and Hemming, 2005).
200 Overall, we believe that the apparent $\delta^{11}B$ offset generated by the N-TIMS method does
201 not invalidate its ability to yield reliable pH records because the offset is compensated for
202 at the calibration stage involving empirical culture experiments with the foraminifer
203 species under consideration.

204 The incorporation of $B(OH)_4^-$ into foraminifer carbonate follows the equilibrium
205 expression (Hemming and Hanson, 1992):

206 $$CaCO_3 + B(OH)_4^- \leftrightarrow Ca(HBO_3) + HCO_3^- + H_2O \quad [1]$$

207 and the surface water B/Ca ration can therefore be expressed as (Yu et al., 2007):

208 $$[B/Ca]_{CaCO3} = K_D \, . \, [B(OH)_4^-/HCO_3^-]_{seawater} \quad [2]$$

209 where the distribution coefficient (K_D) is dependent on temperature and the $[B(OH)_4^-$
210 $/HCO_3^-]_{seawater}$ is pH dependent. Preliminary studies on a limited data set (Yu, 2006)
211 suggest that K_D for *G. sacculifer* follows a similar temperature relationship to *G. inflata*,
212 which has been constrained from core top studies, and shows K_D increasing with
213 temperature (Yu et al., 2007). However, in a down core study from the Caribbean Sea,
214 Foster (2008) observed K_D for *G. sacculifer* decreasing with increasing temperature.
215 More recently, Tripati et al. (2009) concluded that K_D for *G. sacculifer* was only weakly
216 dependent on temperature. The pH values calculated from the K_D values derived from
217 Yu et al. (2007) and Foster (2008) are illustrated in Figures 4b and 4c, respectively.

Although the records are not identical, the pH values derived from the $\delta^{11}B$ data and those derived from B/Ca ratios using the Yu et al. (2007) K_D values show broadly similar trends; with pH values of ~8.2 between 29 to 22 ka, followed by a decrease to values of ~8.05-8.10 between 16-9 ka. In contrast, the pH values derived from the B/Ca ratios using the K_D values of Foster (2008) show essentially constant pH values of ~8.15-8.20 over the entire time span.

4. Calculation of surface water pCO_2 and cross-calibration of the proxies

The seawater carbonate system has two degrees of freedom (Zeebe and Wolf-Gladrow, 2001). Hence, in addition to pH an additional parameter is required to calculate surface water pCO_2. One method is to use alkalinity, and assume that alkalinity is proportional to salinity variations resulting from changes the volume of the oceans as monitored by sea level variations (Waelbroeck et al., 2002; Palmer and Pearson, 2003). This approach yields a change of <20 μeq/kg in alkalinity between 30-5 ka (the age range considered in this study). However, it is important to note that the calculated pCO_2 is relatively insensitive to reasonable uncertainties in alkalinity. For example, an uncertainty of ±50 μeq/kg in alkalinity leads to an uncertainty of only ±5.5 ppm in pCO_2 at a pH of 8.2, using the carbonate equilibrium constants described in Zeebe and Wolf-Gladrow (2001) – which is well within the analytical error of measurements of either the $\delta^{11}B$ value or B/Ca ratio (typically ±20 ppm in both cases). Similarly, uncertainties of ±2^{o}C in temperature and ±1 salinity unit, lead to corresponding uncertainties of only ±3.2 and ±2.5 ppm CO_2, respectively, when considering the dependence of carbonate and borate equilibria on these parameters.

241 The surface water pCO_2 values calculated from the pH reconstructions from the
242 $\delta^{11}B$ values and B/Ca ratios, and assuming alkalinity proportional to ocean volume as
243 given by sea level variations (Waelbroeck et al., 2002) are illustrated in Figure 5. Again,
244 records derived from the $\delta^{11}B$ and Yu et al. (2007) K_D values are more similar to one
245 another than the pCO_2 values derived from the Foster (2008) K_D values.

246 In addition to calculating pCO_2 independently from both the $\delta^{11}B$ and B/Ca
247 proxies, they can be combined to yield pCO_2 values. The $\delta^{11}B$ values can then be used to
248 derive pH, and hence $[B(OH)_4^-]$, and the B/Ca values substituted into equation [2] to
249 yield $[HCO_3^-]$. With two degrees of freedom defined within the carbonate system it is
250 then possible to calculate pCO_2 without assuming any value for alkalinity (Foster, 2008).
251 The surface water pCO_2 values calculated from the combined use of the B/Ca and $\delta^{11}B$
252 proxies are illustrated in Figure 6. The close agreement between the two curves derived
253 from the different formulations of the B/Ca K_D-temperature relationship clearly illustrate
254 the dominant role played by pH (as defined by the $\delta^{11}B$ data) in defining pCO_2 values.
255 This observation suggests that the B/Ca proxy does not greatly aid in constraining surface
256 water pCO_2, regardless of the nature of the K_D-temperature relationship.

257 Surface water pCO_2 records can also be reconstructed from the alkenone carbon
258 isotope composition ($\delta^{13}C_{alk}$) based on the records of carbon isotope fractionation during
259 photosynthetic carbon fixation (Pagani, 2002). In addition to $\delta^{13}C_{alk}$, this method
260 requires a record of the $\delta^{13}C$ of dissolved inorganic carbon ($\delta^{13}C_{DIC}$) (derived here from
261 the $\delta^{13}C$ of *G. ruber*) and dissolved phosphate $[PO_4^{3-}]$ (derived here from the Cd/Ca ratio
262 of *G. sacculifer* (Elderfield and Rickaby, 2000)).

263 The relevant equations are (Pagani, 2002):

$$\varepsilon_{p37.2} = [(\delta d + 1000/\delta p + 1000)-1] \times 10^3 \quad [3]$$

Where, δd is the $\delta^{13}C$ of the inorganic carbonate ($\delta^{13}C_{DIC}$) in the mixed layer (obtained from $\delta^{13}C$ *G. ruber*), and δp is the $\delta^{13}C$ of the haptophyte organic matter enriched by 4.2‰ relative to alkenone $\delta^{13}C$. Surface water pCO_2 can then be calculated from:

$$\varepsilon_{p37.2} = \varepsilon_f - b/[CO_2(aq)] \quad [4]$$

Where, ε_f is the carbon isotope fractionation due to carboxylation (25-27‰, Popp et al., 1998; Goericke et al., 1994).

$$b = \{(118.52[PO_4^{3-}]) + 84.07\}/(25 - \varepsilon_{p37.2}) \quad [5]$$

Values for pCO2 are then obtained from the appropriate carbonate ion equilibrium constants (Zeebe and Wolf-Gladrow, 2001), with salinity obtained from the sea level curve and temperature from the $U^{k'}_{37}$-index measured in the alkenones.

A 1‰ uncertainty $\delta^{13}C_{DIC}$ in would lead to a ~25 ppm uncertainty in the calculated pCO_2. This level of uncertainty is similar to the 0.5-1.5‰ offset in $\delta^{13}C$ values that are observed in foraminifer species hosting algal symbionts (such as *G. ruber*), hence variations of this magnitude have a minimal impact on estimated pCO_2 from alkenones (Pagani et al., 1999). By comparison, a typical uncertainty of ±10% in the Cd/Ca would lead to a similar level of uncertainty in the calculated $[PO_4^{3-}]$ concentration and a 15 ppm uncertainty in the calculated pCO_2 value. The surface water pCO_2 values calculated utilizing this approach is illustrated in Figure 7.

The pCO_2 values reconstructed from the $\delta^{11}B$ record (Fig. 5a) and the alkenone record (Fig. 7) yield broadly similar results – with calculated pCO_2 values rising from ~300 ppm between 29-17 ka, to maximum values of ~400 ppm between 16-12 ka, before falling back to values of ~350 ppm in the most recent samples. These two

reconstructions are entirely independent, and are not based on any shared data (other than the age model). This observation is supportive of the hypothesis that the $\delta^{11}B$ and $\delta^{13}C_{alk}$ proxies are capable of yielding reliable reconstructions of surface water pCO_2 values when used in appropriate combination with other proxies for temperature, $\delta^{13}C_{DIC}$ and nutrient concentrations.

As noted above, Cd/Ca ratios of *G. sacculifer* can be used to reconstruct surface water $[PO_4^{3-}]$ (Elderfield and Rickaby, 2000). Alternatively, surface water $[PO_4^{3-}]$ can be reconstructed if the surface water pCO_2 values reconstructed from the $\delta^{11}B$ proxy are assumed to be reliable, and then inverting the alkenone data to derive the $[PO_4^{3-}]$ values required to achieve the same pCO_2 values. Again, the two independent $[PO_4^{3-}]$ reconstructions show broadly consistent patterns, with relatively low concentrations in the period 29-16 ka, a peak at ~14-11 ka, and a return to lower values in the most recent samples (Fig. 8).

5. Discussion

It has been estimated that there is currently a flux of ~70 x 10^{12} g C yr^{-1} to the atmosphere from the Arabian Sea, of which the ASM contributes ~60% (Sarma, 2003). This flux of CO_2 is second only to the eastern equatorial Pacific upwelling system as an oceanic source of atmospheric CO_2 (Takahashi et al., 2002; Sarma, 2003). Figure 9 illustrates the pooled pCO_2 surface water reconstructions from the $\delta^{11}B$ and $\delta^{13}C_{alk}$ proxies, together with the variations in ΔpCO_2 (the difference between the pCO_2 of the surface waters and contemporaneous atmosphere, as derived from the ice core record (Indermuhle et al., 1999; Smith et al., 1999)). It is apparent that this area of the oceans

has been a source of CO_2 to the atmosphere throughout the entire time interval covered by this study, although the magnitude of this flux has varied. It is noteworthy that the maxima in pCO_2 and ΔpCO_2 are coincident with the second pulse of the rapid post glacial increase in atmospheric CO_2 (Monnin et al., 2004), hence it is possible that increased intensity of the ASM may have contributed to this change.

In addition to ΔpCO_2, the flux of CO_2 between surface seawater and the atmosphere depends on the CO_2 gas transfer velocity, which is in turn dependent on the surface wind speed (Wanninkhof, 1992). Because surface wind speeds are greater over the Arabian Sea during periods of enhanced monsoon activity (Schott and McCreary, 2001), the magnitude of the CO_2 flux from the Arabian Sea to the atmosphere would likely have been greater than implied by the change in ΔpCO_2 alone. It is important to note, however, that the net flux of CO_2 to the atmosphere is also dependent on any enhanced biological carbon fixation and burial associated arising from the concomitant high nutrient concentrations of the upwelled water (for example, as illustrated by the higher surface water [PO_4^{3-}] shown in Fig. 8). Indeed, the present day Arabian Sea is an area of significant biological drawdown of surface water CO_2 (Takahashi et al., 2002). However, the amount of organic carbon preserved in NIOP464 sediments is actually lower during the period of high pCO_2 concentrations (Fig. 9e) (Reichart et al., 1997; 1998). Ivanova et al. (2003) suggest that this may be due to reduced primary productivity in the northern Arabian Sea, but Schenau et al. (2005) also noted that there was a disconnect between the burial efficiency of phosphorus and productivity in the Arabian Sea during the Late Quaternary, that was due in part to fluctuations in bottom water oxygen concentrations. Regardless of the mechanism, it is apparent that high surface

333 water pCO_2 concentrations generated from increased intensity of the ASM did not result
334 in a concomitant increase in burial of organic carbon. Hence, the increased surface water
335 pCO_2 concentrations likely led a net increase in the flux of CO_2 to the atmosphere during
336 ~11-18 ka.

337 The potential magnitude of the effect of enhanced ASM intensity on atmospheric
338 CO_2 levels may be gauged by comparison with the present day. Fossil fuel burning and
339 cement manufacture averaged ~6 x 10^{15} g C yr^{-1}, leading (among other causes) to a rise of
340 ~0.8 ppm yr^{-1} in atmospheric CO_2 (Boden and Marland, 2009; Keeling et al., 2009). The
341 present day CO_2 flux to the atmosphere from the Arabian Sea due to the ASM is ~40 x
342 10^{12} g C yr^{-1}, arising from a ΔpCO_2 of ~100 ppm (Sarma, 2003). If the CO_2 flux scales
343 directly with ΔpCO_2, the average ΔpCO_2 of 140 ppm between ~11-18 ka would
344 correspond to an increase of ~25 x 10^{12} g C yr^{-1} in the CO_2 flux arising from the ASM.
345 By analogy with the present day rise in atmospheric CO_2 levels, this would suggest the
346 contribution of the more intense ASM to rising atmospheric CO_2 levels between 11-18 ka
347 was ~0.003 ppm yr^{-1}, compared to an average rise of ~0.010 ppm yr^{-1} over this interval
348 (Monnin et al., 2004; Fig. 9c).

349 There has been considerable debate regarding the relative timing of the ASM and
350 the orbitally-driven temporal variations in the strength of insolation over the Tibetan
351 plateau (e.g., Ruddiman, 2006; Clemens and Prell, 2007). While this study only covers a
352 relatively brief period, it does cover most of a full precession cycle and, by dint of
353 covering the most recent cycle, it is the most accurately dated period of the marine
354 record.

355 Figure 10 is a compilation of the pCO_2 and $[PO_4^{3-}]$ records generated in this study,
356 together with other marine and terrestrial records spanning the relevant time interval.
357 Also included in Figure 10 is the summer insolation record over the Tibetan plateau (Fig.
358 10c) (Huybers, 2006) and the Asian Summer Monsoon Stack (SMS) (Fig. 10d) generated
359 by Clemens and Prell (2003). The SMS is a compilation of five marine proxies ($\delta^{15}N$,
360 opal mass accumulation rate, percentage abundance of *G. bulloides*, lithogenic grain size,
361 and excess Ba mass accumulation rate) obtained from two sediment cores from the Owen
362 Ridge off the Oman margin (Clemens & Prell, 2003). These proxies were then combined
363 (stacked) and subjected to a principal components analysis to yield the SMS. Over the
364 350,000 time period considered by Clemens and Prell (2003), the SMS lagged the
365 precession-driven, northern hemisphere summer insolation maximum by an average of
366 121^{o}, or 7.7 ka. This lag has been interpreted as being due to a complex interplay
367 between land surface and ocean feedbacks that produce climatic responses that are of the
368 same order as radiative forcing, such that the latent heat influx from the southern
369 hemisphere leads to a delay in the response of the ASM to the rise in insolation (Clemens
370 and Prell, 2003; 2007). This offset is seen clearly in Figure 10 where, for the last
371 precession cycle, the SMS maximum lags the insolation maximum by 3 kyr.
372 In contrast, the oxygen isotope compositions of stalagmites from China extending
373 back to 224 ka, have been used to argue that there is no discernable delay between the
374 intensity of the ASM and northern hemisphere insolation (Wang et al., 2001; Yuan et al.,
375 2005; Wang et al., 2008). Clemens and Prell (2007) countered this observation by
376 arguing that these Chinese speleothems monitor precipitation associated with the East
377 Asian monsoon, that has a West Pacific moisture source, and do not therefore provide a

valid record of the strength of the ASM. However, recent $\delta^{18}O$ data from a stalagmite from Socotra Island, Yemen, which is far removed from the influence of the East Asian monsoon, show close agreement with the Chinese stalagmite data and have been interpreted to suggest that both localities record the isotope record of precipitation, which is in turn driven by the strength of the ASM (Shakun et al., 2007). Although the Socotra record is not complete over the time period considered in this study, Figure 10e clearly shows the $\delta^{18}O$ values decreasing in phase with the rise in insolation (Huybers, 2006) and with the pCO_2 and $[PO_4^{3-}]$ proxy records from this study, but well before the rise in the SMS (Clemens and Prell, 2003).

The Socotra speleothem record also accords with $\delta^{15}N$ data from core NIOP905 from the Somalia margin that shows the strength of the ASM declining after ~ 10 ka (Ivanochko et al., 2005) (Fig. 10f), before the SMS reaches its maximum value. Shakun et al. (2007) noted that both these records contain a strong signal of the Younger Dryas, and suggested that, in addition to changes in insolation, the strength of the ASM was strongly influenced by the extent of northern hemisphere climatic forcing during the last deglaciation.

As noted above, one of the proxies used by Clemens and Prell (2003) to compile the SMS is the excess Ba concentration measured in sediments. In this study, we have extended the Ba/Al record of Reichart et al. (1997) from NIOP464 piston core to 7.6 ka by using sediments from the trigger weight of the piston core, and replotting the data according to the age model of Reichart et al. (1998) (Fig. 10g). Again, the age of the maximum in this proxy coincides with timing of the maximum insolation over the

400 Tibetan plateau during the last deglaciation (Huybers, 2006) and occurs significantly
401 ahead of the peak in the SMS signal (Clemens and Prell, 2003).

402 There are several possible reasons for the apparent discrepancy between the proxy
403 records from this study and others (Wang et al., 2001; Ivanochko et al., 2005; Yuan et al.,
404 2005; Shakun et al., 2007; Wang et al., 2008) that appear to show the AMS in phase with
405 insolation, and the hypothesis that a significant lag exists between the peak in insolation
406 and the strength of the ASM (Clemens and Prell, 2003). It is possible that past variations
407 in the surface water pCO_2 and $[PO_4^{3-}]$ concentrations and Ba/Al ratios at the site of
408 NIOP464 do not directly reflect the intensity of the ASM if, for example, there were
409 temporal variations in the depth from which the upwelled waters were derived and the
410 advection pathway of the upwelled waters into the Arabian Sea. Indeed, variations in
411 both these parameters are seen on an interannual basis in the modern Arabian Sea (Schott
412 and McCreary, 2001). However, if this were the case then it would also call into question
413 the marine records used to generate the SMS index (Clemens and Prell, 2003), and indeed
414 many other marine records of monsoon activity.

415 The time period covered in this study is too short to resolve the long-standing
416 debate regarding the phasing of the ASM with insolation and/or other climate forcing
417 functions over multiple orbital cycles. Nevertheless, the observations presented here are
418 consistent with a recent study which suggests that northern hemisphere climatic controls
419 exhibit a stronger control over ASM intensity when the monsoon is strong, thus
420 explaining the apparent synchronicity between the NIOP 464 ASM proxies and northern
421 hemisphere insolation (Fig. 10), but that southern hemisphere processes exhibit a greater
422 control over ASM intensity when the monsoon is weak (Rohling et al., 2009).

6. Conclusions

We have demonstrated that the $\delta^{11}B$ and $\delta^{13}C_{alk}$ proxies can yield reliable and self consistent reconstructions of surface water pCO_2 when used in combination with other paleoceanographic proxies of temperature (Mg/Ca and $U^{k'}_{37}$-index), $\delta^{13}C_{DIC}$ (from foraminifera $\delta^{13}C$) and nutrient concentrations (from foraminifera Cd/Ca).

These proxies have been applied to sediments separated from the NIOP464 core taken from the Northern Arabian Sea, and show that this area has been a constant source of CO_2 to the atmosphere over the interval 5-29 ka. The magnitude of this source shows considerable variation with time, and was greatest between ~11-17 ka. This period coincides with the time when atmospheric CO_2 levels were rapidly increasing during the last deglaciation.

The reconstructed surface water pCO_2 and $[PO_4^{3-}]$ concentrations show maximum values that are coincident with the maximum in northern hemisphere summer insolation over the Tibetan plateau. The timing of these maxima is consistent with other proxy data from the region from both marine sediment cores and speleothems. In contrast, the data presented here do not support the 3 kyr lag between the timing of the summer monsoon maximum and northern hemisphere summer insolation proposed by Clemens and Prell (2003).

Our observations are consistent with the hypothesis that northern hemisphere climatic forcing functions play a greater role in controlling of the Asian summer monsoon during times of strong monsoons, and that the southern hemisphere factors are more important during times of weak monsoons (Rohling et al., 2009).

Acknowledgements

This study was funded by the 6C program of the EC, and we thank J. Bijma for his role in coordinating this project. JA Milton and J Ossebaar assisted with the analyses. Thanks also to EJ Rohling, GL Foster and H Palike for helpful discussions and feedback. This manuscript was also greatly improved as the result of three constructive anonymous reviews.

References

Abram, N.J., Gagan, M.K., Liu, Z., Hantro, W.S., McCulloch, M.T., Suwargadi, B.W., 2007, Seasonal characteristics of the Indian Ocean Dipole during the Holocene epoch. Nature 445, 299-302.

Agnihotri, R., Dutta, K., Bhushan, R., Somayajulu, B.L.K., 2002, Evidence for solar forcing on the Indian monsoon during the last millenium. Earth Planet. Sci. Lett. 198, 521-527.

Anand, P., Elderfield, H., Conte, M.H., 2003. Calibration of Mg/Ca thermometry in planktonic foraminifera from a sediment trap time series. Paleoceanogr. 18, 1050, doi:10.1029/2002PA000846.

Anderson, R.F., Chase, Z., Fleisher, M.Q., Sachs, J., 2002. The Southern Ocean's biological pump during the Last Glacial Maximum. Deep-Sea Res. II 49, 1909-1938.

Archer, D., Maier-Reimer, E., 1994. Effect of deep-sea sedimentary calcite preservation on atmospheric CO_2 concentration. Nature 367, 260-263.

468 Boden, T., Marland, G., 2009. Global CO_2 emissions from fossil-fuel burning, cement
469 manufacture and gas flaring: 1751-2006. doi 10.3334/CDIAC/00001.
470 Brassell, S.C., 1993. Applications of biomarkers for delineating marine paleoclimatic
471 fluctuations during the Pleistocene. In: M.H. Engel, S.A. Macko (Eds.), Organic
472 Geochemistry, Plenum Press, New York, 699-738.
473 Brassell, S.C., Eglinton, G., Marlowe, I.T., Pflaumann, U., Sarntheim, M., 1986.
474 Molecular stratigraphy – a new tool for climatic assessment. Nature, 320, 129-133.
475 Broecker, W.S., 1982. Glacial to interglacial changes in ocean chemistry. Prog. Oceangr.
476 2, 151-197.
477 Cayre, O., Beaufort, L., Vincent, E., 1999. Paleoproductivity in the Equatorial Indian
478 Ocean for the last 260,000 yr: A transfer function based on planktonic foraminifera.
479 Quat. Sci. Rev. 18, 839-857.
480 Clemens, S.C., Prell, W.L., 2003. A 350,000 year summer-monsoon multi-proxy stack
481 from the Owen Ridge, Northern Arabian Sea. Mar. Geol. 201, 35-51.
482 Clemens, S.C., Prell, W.L., 2007. The timing of orbital-scale Indian monsoon changes.
483 Quat. Sci. Rev. 26, 275-278.
484 Curry, W.B., Ostermann, D.R., Guptha, M.V.S., Ittekkot, V., 1992. Foraminferal
485 production and monsoonal upwelling in the Arabian Sea: evidence from sediment
486 traps (suppl. data). Geol. Soc. Lond. Spec. Publ. 64, 93-106.
487 Elderfield, H., Rickaby, R.E.M., 2000. Oceanic Cd/P ratio and nutrient utilization in the
488 glacial Southern Ocean. Nature 405, 305-310.

489 Foster, G.L., 2008. Seawater pH, pCO_2 and [CO_3^{2-}] variation in the Caribbean Sea over
490 the last 130 kyr: A boron isotope and B/Ca study of planktic foraminifera. Earth
491 Planet. Sci. Lett. 271, 254-266.
492 Goericke, R., Montoya, J.P., Fry, B., 1994, Physiology of isotope fractionation in algae
493 and cyanobacteria, in Stable Isotopes in Ecology (Lajtha K., Michener B. eds.), pp.
494 187–221, Blackwell, Malden, Mass.
495 Hemming, N.G., Hanson, G.N., 1992. Boron isotopic composition and concentration in
496 modern marine carbonates. Geochim. Cosmochim. Acta 56, 537-543.
497 Herzschuh, U., 2006, Palaeo-moisture evolution in monsoonal Central Asia during the
498 last 50,000 years. Quat. Sci. Rev. 25, 163-178.
499 Hönisch, B., Bijma, J., Russell, A.D., Spero, H.J., Palmer, M.R., Zeebe, R.E., Eisenhauer,
500 A., 2003, The influence of symbiont photosynthesis on the boron isotopic
501 composition of foraminifera shells. Mar. Micropaleontol. 49, 87-96.
502 Hönisch, B., Hemming, N.G., 2005. Surface ocean pH response to variations in pCO_2
503 through two full glacial cycles. Earth Planet. Sci. Lett. 236, 305-314.
504 Honjo, S., Dymond, J., Prell, W., Ittekkot, V., 1999. Monsoon-controlled export fluxes to
505 the interior of the Arabian Sea, Deep Sea Res. II 46, 1859-1902.
506 Huybers, P., 2006. Early Pleistocene glacial cycles and the integrated summer insolation
507 forcing. Science 313, 508-511.
508 Imbrie, J., Hays, J.D., Martinson, D.G., McIntyre, A., Mix, A.C., Morley, J.J., Pisias,
509 N.G., Prell, W.L., Shackleton, N.J., 1984. The orbital theory of Pleistocene climate:
510 support from a revised chronology of the marine $\delta^{18}O$ record. In: A.L. Berger, J.

511 Imbrie, J. Hays, G. Kukla, B. Saltzman (eds.), Milankovitch and Climate, Part I,
512 Reidel Dordrecht, 269-305.
513 Indermühle, A., Stocker, T.F., Joos, F., Fischer, H., Smith, H.J., Wahlen, M., Deck, B.,
514 Mastroianni, D., Tschumi, J., Blunier, T., Meyer, R., Stauffer, B., 1999. Holocene
515 carbon-cycle dynamics based on CO_2 trapped in ice at Taylor Dome, Antarctica.
516 Nature 398, 121-126.
517 Ivanochko, T.S., Ganeshram, R.S., Brummer, G.J.A., Ganssen, G., Jung, S.J.A., Moreton,
518 S.G., Kroon, D., 2005. Variations in tropical convection as an amplifier of global
519 climate change at the millennial scale. Earth Planet. Sci. Lett. 235, 302-314.
520 Ivanova, E., Schiebel, R., Singh, A.D., Schmiedl, G., Niebler, H.S., Hemleben, C., 2003.
521 Primary production in the Arabian Sea during the last 135,000 years. Palaeogeog.
522 Palaeoclim. Palaeoecol. 197, 61-82.
523 Keeling, R.F., Piper, S.C., Bollenbacher, A.F., Walker, J.S., 2009. Atmospheric CO_2
524 records from sites in the SIO air sampling network. In: Trends: A Compendium of
525 Data on Global Change. CDIAC, ORNL, US Dept. Energy, Oak Ridge, TN, USA.
526 (cdiac.ornl.gov/trends/co2/sio-mlo.html).
527 Klochko, K., Kaufman, A.J., Yoa, W., Byrne, R.H., Tossell, J.A., 2006. Experimental
528 measurement of boron isotope fractionation in seawater. Earth Planet. Sci. Lett. 248,
529 261-270.
530 Lu, R., Dong, B., Ding, H., 2006, Impact of the Atlantic Multidecadal Oscillation on the
531 Asian summer. Geophys. Res. Lett. 33, L24701.

532 Martinson, D.G., Pisias, N.G., Hays, J.D., Imbrie, J., Moore, T.C., Shackleton, N.J.,
533 1987. Age dating and the orbital theory of the ice ages: development of a high-
534 resolution 0-300,000 year chronostratigraphy. Quat. Res. 27, 1-29.
535 Monnin, E., Steig, E.J., Siegenthaler, U., Kawamura, K., Schwander, J., Stauffer, B.,
536 Stocker, T.F., Morse, D.L., Barnola, J.M., Bellier, B., Raynaud, D., Fischer, H., 2004.
537 Evidence for substantial accumulation rate variability in Antarctica during the
538 Holocene through synchronization of CO_2 in the Taylor Dome, Dome C and DML ice
539 cores. Earth Planet. Sci. Lett. 224, 45-54.
540 Pagani, M., Arthur, M.A., Freeman, K.H., 1999, Miocene evolution of atmospheric
541 carbon dioxide. Paleoceanogr. 14, 272-292.
542 Pagani, M., 2002. The alkenone-CO_2 proxy and ancient atmospheric carbon dioxide.
543 Trans. Roy. Soc. Lond. Ser. A 360, 575-602.
544 Palmer, M.R., Pearson, P.N., Cobb, S.J., 1998. Reconstructing past ocean pH-depth
545 profiles. Science 282, 1468-1471.
546 Palmer, M.R., Pearson, P.N., 2003. A 23,000-year record of surface ocean water pH and
547 pCO_2 in the Western equatorial Pacific Ocean. Science 300, 480-482.
548 Peeters, F.J.C., Brummer, G.J.A., 2002. The seasonal and vertical distribution of living
549 planktic foraminifera in the NW Arabian Sea. Geol. Soc. Lond. Spec. Publ. 195, 463-
550 497.
551 Popp, B.N., Laws, E.A., Bidigare, R.R., Dore, J.E., Hanson, K.L., Wakeham, S.G., 1998,
552 Effect of phytoplankton cell geometry on carbon isotopic fractionation, Geochim.
553 Cosmochim. Acta 62, 69-77.

554 Prahl, F.G., Dymond, J., Sparrow, M.A., 2000. Annual biomarker record for export
555 production in the central Arabian Sea. Deep Sea Res. II 47, 1581-1604.
556 Prell, W.L., Curry, W.B., 1981. Faunal and isotopic indices of monsoonal upwelling:
557 western Arabian Sea. Oceanol. Acta 4, 91-98.
558 Reichart, G.J., den Dulk, M., Visser, H.J., van der Weijden, C.H., Zachariasse, W.J.,
559 1997. A 225 kyr record of dust supply, paleoproductivity and the oxygen minimum
560 zone from the Murray Ridge (northern Arabian Sea). Palaeogeog. Palaeoclimat.
561 Palaeoecol. 134, 149-169.
562 Reichart, G.J., Lourens, J., Zachariasse, W.J., 1998. Temporal variability in the northern
563 Arabian Sea Oxygen Minimum Zone (OMZ) during the last 225,000 years.
564 Paleoceanogr. 13, 607-621.
565 Rodwell, M.J., 1997. Breaks in the Asian monsoon: the influence of Southern
566 Hemisphere weather systems. J. Atmos. Sci., 54, 2597-2611.
567 Rohling, E.J., Liu, Q.S., Roberts, A.P., Stanford, J.D., Rasmussen, S.O., Langen, P.L.,
568 Siddall, M., 2009. Controls on the East Asian monsoon during the last glacial cycle,
569 based on comparison between Hulu Cave and polar ice-core records. Quat. Sci. Rev.
570 (in press).
571 Ruddiman, W.F., 2006. What is the timing of orbital-scale monsoon changes? Quat. Sci.
572 Rev. 25, 657-658.
573 Sanyal, A., Bijma, J., Spero, H., Lea, D.W., 2001. Empirical relationship between pH and
574 the boron isotopic composition of *Globigerinoides sacculifer*: Implications for the
575 boron isotope paleo-proxy. Paleoceanogr. 16, 515-519.

576 Sarma, V.V.S.S., 2003. Monthly variability in surface pCO_2 and net air-sea CO_2 flux in
577 the Arabian Sea. J. Geophys. Res. 108, 3255 doi:10.1029/2001JC001062.
578 Schenau, S.J., Reichart, G.J., de Lange, G.J. 2005. Phosphorus burial as a function of
579 paleoproductivity and redox conditions in Arabian Sea sediments. Geochim.
580 Cosmochim. Acta 69, 919-931.
581 Schouten, S., Breteler, W.C.M., Blokker, P., Schogt, N., Rijpstra, W.I.C., Grice, K., Baas,
582 M., Damsté, J.S.S., 1998. Biosynthetic effects on the stable carbon isotopic
583 compositions of algal lipids: Implications for deciphering the carbon isotopic
584 biomarker record. Geochim. Cosmochim. Acta 62, 1397-1406.
585 Schouten, S., Hoefs, M.J.L., Damsté, J.S.S., 2000. A molecular and stable carbon isotope
586 study of lipids in late Quaternary sediments from the Arabian Sea. Organic Geochem.
587 31, 509-521.
588 Schott, F.A., McCreary, J.P., 2001. The monsoon circulation of the Indian Ocean. Progr.
589 Oceanogr. 51, 1-123.
590 Schulte, S., Müller, P.J., 2001. Variations of sea surface temperature and primary
591 productivity during Heinrich and Dansgaard-Oeschger events in the northern Arabian
592 Sea. Geo-Mar. Lett. 21, 168-175.
593 Shakun, J.D., Burns, S.J., Fleitmann, D., Kramers, J., Matter, A., Al-Subary, A., 2007. A
594 high-resolution, absolute-dated deglacial speleothem record of Indian Ocean climate
595 from Socotra Island, Yemen. Earth Planet. Sci. Lett. 259, 442-456.
596 Smith, H.J., Fischer, H., Wahlen, M., Mastroianni, D., Deck, B., 1999. Dual modes of the
597 carbon cycle since the Last Glacial Maximum. Nature 400, 248-250.

598 Takahashi, T., Sutherland, S.C., Sweeney, C., Poisson, A., Metzl, N., Tilbrook, B., Bates,
599 N., Wanninkhof, R., Feely, R.A., Sabine, C., Olafsson, J., Nojiri, Y., 2002. Global
600 sea-air CO_2 flux based on climatological surface ocean pCO_2, and seasonal biological
601 and temperature effects. Deep-Sea Res. II 49, 1601-1622.
602 Waelbroeck, C., Labeyrie, L., Michel, E., Duplessy, J.C., McManus, J.F., Lambeck, K.,
603 Balbon, E., Labacherie, M., 2002. Sea-level and deep water temperature changes
604 derived from benthic foraminifera isotopic records. Quat. Sci. Rev. 21, 295-305.
605 Wang, P., Clemens, S., Beaufort, L., Braconnot, P., Gansen, G., Jian, Z., Kershaw, P.,
606 Sarnthein, M., 2005. Evolution and variability of the Asian monsoon system: state of
607 the art and outstanding issues. Quat. Sci. Rev. 24, 595-629.
608 Wang, Y.J., Cheng, H., Edwards, R.L., An, Z.S., Wu, J.Y., Shen, C.C., Dorale, J.A.,
609 2001. A high-resolution absolute-dated Late Pleistocene monsoon record from Hulu
610 cave, China. Science 294, 2345-2348.
611 Wang, Y., Cheng, H., Edwards, R.L., Kong, X., Shao, X., Chen, S., Wu, J., Jiang, X.,
612 Wang, X., An, Z., 2008. Millenial- and orbital-scale changes in the East Asian
613 monsoon over the past 224,000 years. Nature 224, 1090-1093.
614 Wanninkhof, R., 1992. Relationship between wind speed and gas exchange. J. Geophys.
615 Res. 97, 7373-7382.
616 Wyrtki, K., 1973. Physical Oceanography of the Indian Ocean. Berlin, Springer-Verlag,
617 18-36.
618 Yu, J.M., Day, J. Greaves, M., Elderfield, H., 2005. Determination of multiple
619 element/calcium ratios in foraminiferal calcite by quadrupole ICP-MS. Geochem.
620 Geophys. Geosys. 6, Q08P01.

621 Yu, J.M., 2006, Boron concentration in foraminifera as a proxy for glacial-interglacial
622 change in the oceanic carbonate system. Ph.D. thesis, 155 pp., Univ. Cambridge, U.K.
623 Yu, J.M., Elderfield, H., Honisch, B., 2007. B/Ca in planktonic foraminifera as a proxy
624 for surface water pH. Paleoceanogr. 22, doi.org/10.1029/2006PA001347.
625 Yuan, D., Cheng, H., Edwards, R.L., Dykoski, C.A., Kelly, M.J., Zhang, M., Qing, J.,
626 Lin, Y., Wang, Y., Wu, J., Dorale, J.A., An, Z., Cai, Y., 2004. Timing, duration, and
627 last transition of the last interglacial Asian monsoon. Science 304, 575-578.
628 Zeebe, R., Wolf-Gladrow, D., 2001. CO_2 in Seawater: Equilibrium, Kinetics, Isotopes.
629 (Elsevier, Amsterdam).

630 **Figure Captions**

631 Figure 1.

632 Sediment properties used in cross calibrating trigger weight core (open circles) and piston
633 core (black circles) for NIOP464.

634

635 Figure 2.

636 a) Species fluxes of *G. bulloides* (triangles, dotted line), *G. sacculifer* (diamonds,
637 solid line) and *G. ruber* (squares, dashed line) (>150 μm) in the western Arabian
638 Sea (Curry et al., 1992). Note, because of the large differences in the numbers of
639 the three species, for ease of comparison the data are plotted as the daily fluxes
640 (for the 12-13 days of each interval) divided by the average daily flux for each
641 species over the sampling interval. Curry et al. (1992) ascribe the absence of data
642 in some of inter-monsoon periods to insufficient material in the sediment traps to
643 allow for meaningful calculations.

644 b) Flux of alkenones (solid line) and $CaCO_3$ (dashed line) in the western Arabian Sea
645 (Prahl et al., 2000) expressed as daily fluxes (for the 12-13 days of each interval)
646 divided by the average daily flux over the sampling interval.

647

648 Figure 3.

649 Sea surface temperatures reconstructed from $U^{k'}_{37}$-index (circles) and Mg/Ca ratios of *G.*
650 *sacculifer* (squares). The data are plotted as 3 point running means with 1σ error bars.
651 The average age resolution is ±0.5 kyr.

652

653 Figure 4.

654 a) Surface water pH reconstructed from $\delta^{11}B$ (squares).

655 b) Surface water pH reconstructed from B/Ca (circles) using K_D-temperature
656 relationship of Yu et al. (2007).

657 c) Surface water pH reconstructed from B/Ca (diamonds) using K_D-temperature
658 relationship of Foster (2008).

659 The data are plotted as 3pt running means with 1σ error bars. The average age
660 resolution is ±0.5 kyr.

661

662 Figure 5.

663 a) Surface water pCO_2 values calculated from pH values derived from $\delta^{11}B$ values
664 measured in *G. sacculifer.*

665 b) Surface water pCO_2 values calculated from pH values derived from B/Ca values
666 measured in *G. sacculifer* and K_D values of Yu et al. (2007).

667 c) Surface water pCO_2 values calculated from pH values derived from B/Ca values
668 measured in *G. sacculifer* and K_D values of Foster (2008).

669 In all three cases alkalinity is assumed to be proportional to salinity as derived from
670 variations in sea level. The data are plotted as 3 point running means with 1σ error
671 bars.

672

673 Figure 6.

Surface water pCO_2 values (3 point running means with 1σ error bars) calculated from combined use of the $\delta^{11}B$ and B/Ca proxies. a) Using the Yu et al. (2007) B/Ca K_D-temperature relationship. b) Using the Foster (2008) B/Ca K_D-temperature relationship.

Figure 7.

Surface water pCO_2 values (3 point running means with 1σ error bars) calculated from combined use of the $\delta^{13}C_{alk}$ and $\delta^{13}C_{DIC}$ and Cd/Ca proxies.

Figure 8.

Surface seawater [PO_4^{3-}] concentrations reconstructed from Cd/Ca ratios of *G. sacculifer* (circles), inversion of the alkenone data (squares) (see text for details), and 3 pt running mean of both reconstructions with 1σ error bars. The average age resolution is ±0.5 kyr.

Figure 9.

a) 3pt running mean of the pooled surface water pCO_2 values calculated from the two methods discussed in the text.
b) 3 pt running mean of the ΔpCO_2 between pCO_2 of surface waters and contemporaneous atmosphere (Indermuhle et al., 1999; Smith et al., 1999).
c) Rate of change of atmospheric CO_2 as determined from a 7pt running mean of high resolution data from Antarctic ice cores (Monnin et al., 2004).
d) Primary productivity variations in the northern Arabian Sea as reconstructed from application of principal component analysis and transfer functions to planktic foraminifera assemblages (Ivanova et al., 2003).

697 e) Percentage organic carbon in sediments from NIOP 464 sediment core (Reichart
698 et al., 1997; 1998).
699
700 Figure 10.
701 a) 3 point running mean (1σ error bars) of pCO_2 values of surface seawater.
702 b) 3 point running mean (1σ error bars) of $[PO_4^{3-}]$ levels of surface seawater.
703 c) Summer insolation variations at 30^oN (Huybers, 2006).
704 d) Arabian Sea summer monsoon stack (SMS) (Clemens and Prell, 2003).
705 e) Socotra stalagmite $\delta^{18}O$ record (Shakun et al., 2007).
706 f) $\delta^{15}N$ record from NIOP905 sediment core (Ivanochko et al., 2005).
707 g) Ba/Al ratios of sediments from NIOP464 sediment core.
708 The composite pCO_2 and PO_4 records obscure the Younger Dryas and Heinrich events
709 seen in the Somalia margin proxies, but as none of these high resolution events are seen
710 in the individual proxy records measured at NIOP464, except for the physical properties
711 (Fig. 1), this suggests that the lower sedimentation rate open ocean site at NIOP464 tends
712 to average out conditions seen in the higher sedimentation rate margin sites.

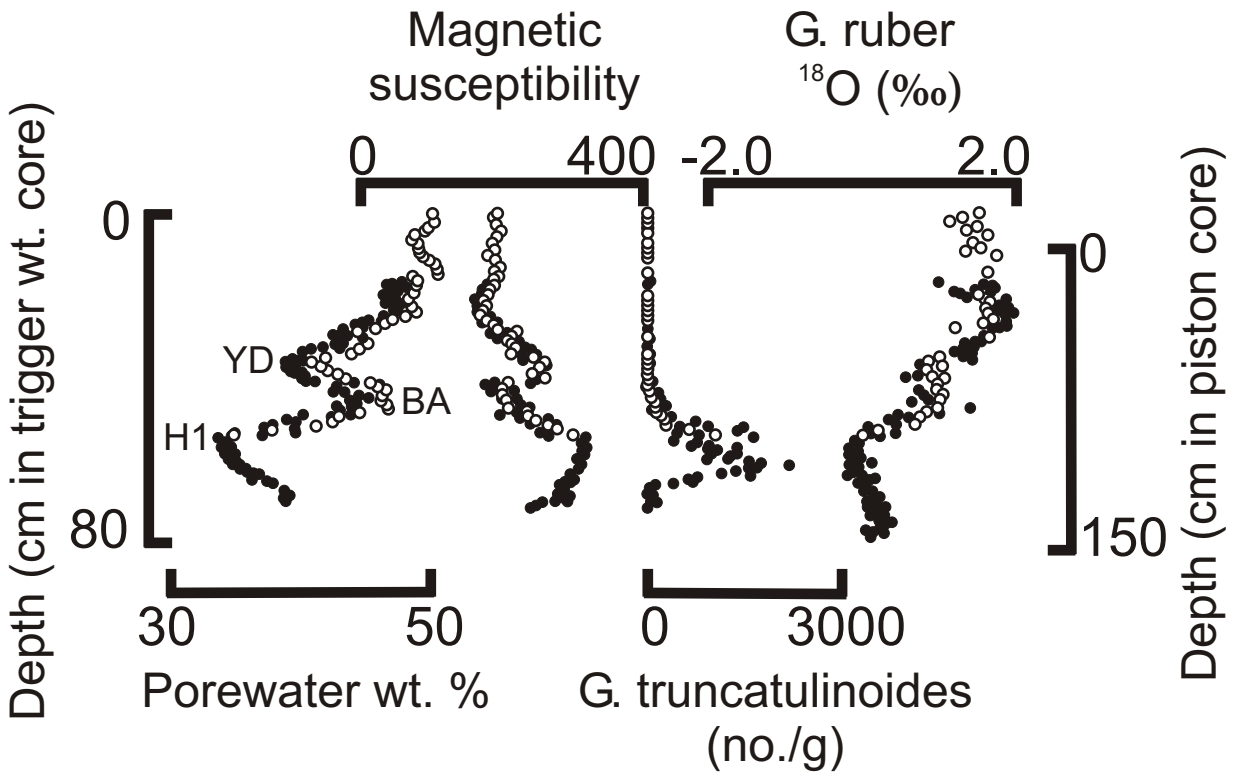
Magnetic
susceptibility
G. ruber
18O (‰)
0
400
-2.0
2.0
0
80
0
150
YD
BA
H1
Depth (cm in trigger wt. core)
Depth (cm in piston core)
30
50
0
3000
Porewater wt. %
G. truncatulinoides
(no./g)

Figure 1

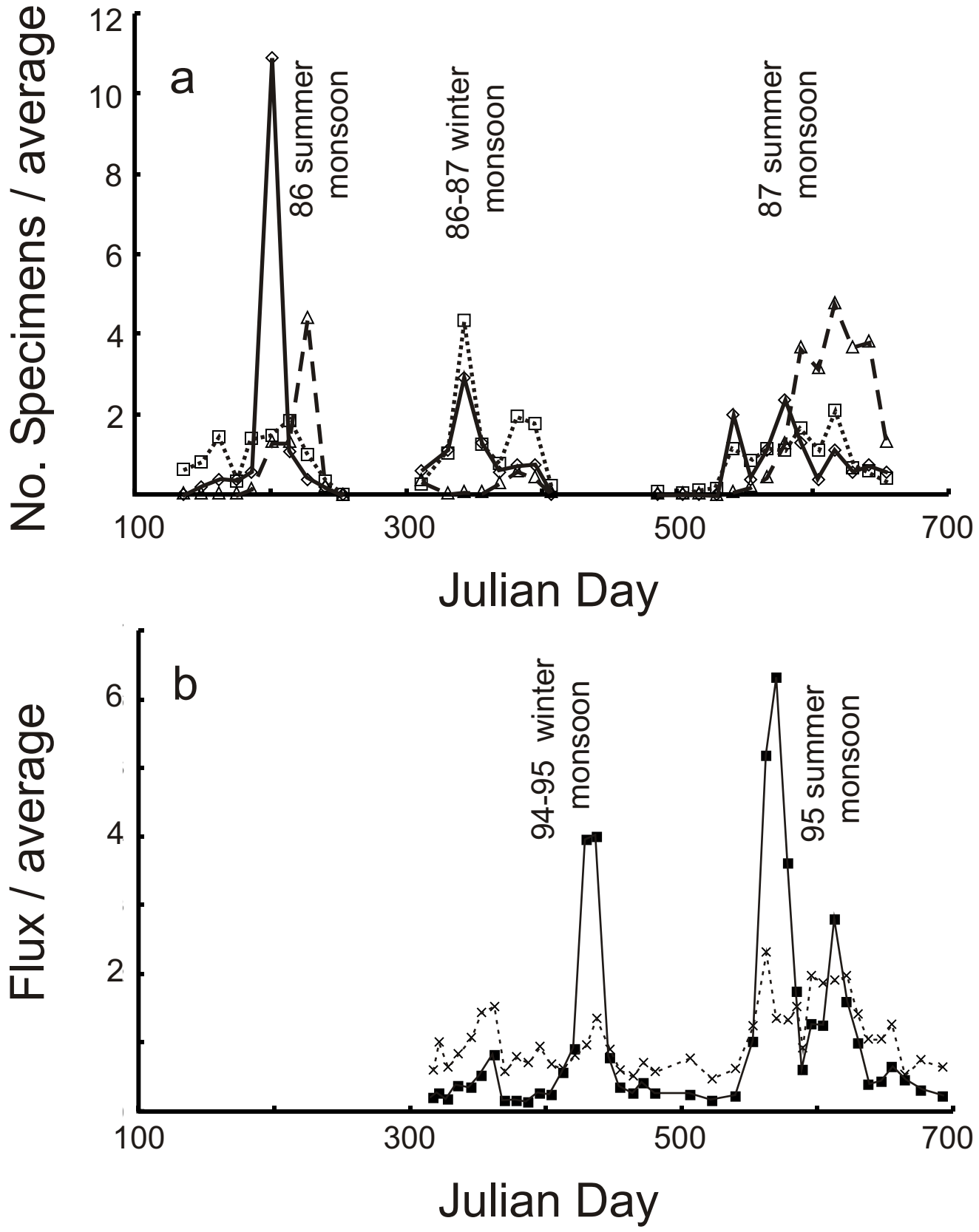
a
No. Specimens / average
12
10
8
6
4
2
86 summer monsoon
86-87 winter monsoon
87 summer monsoon
100
300
500
700
Julian Day
b
Flux / average
6
4
2
94-95 winter monsoon
95 summer monsoon
100
300
500
700
Julian Day

Figure 2

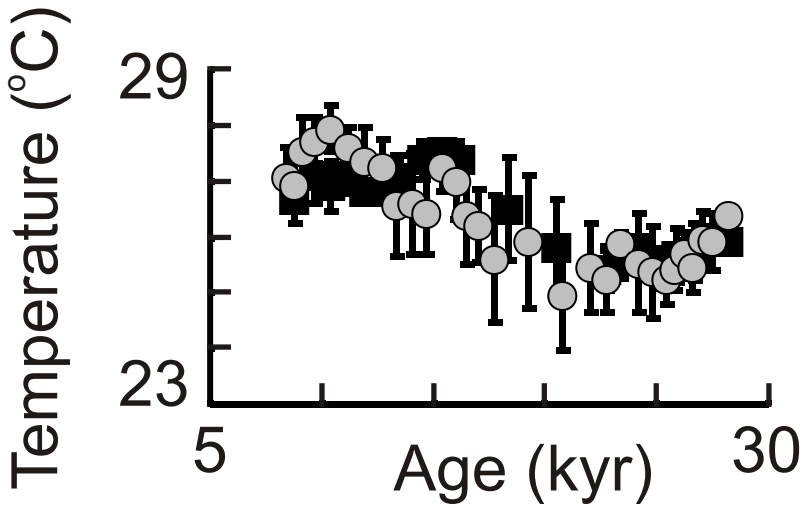

Figure 3

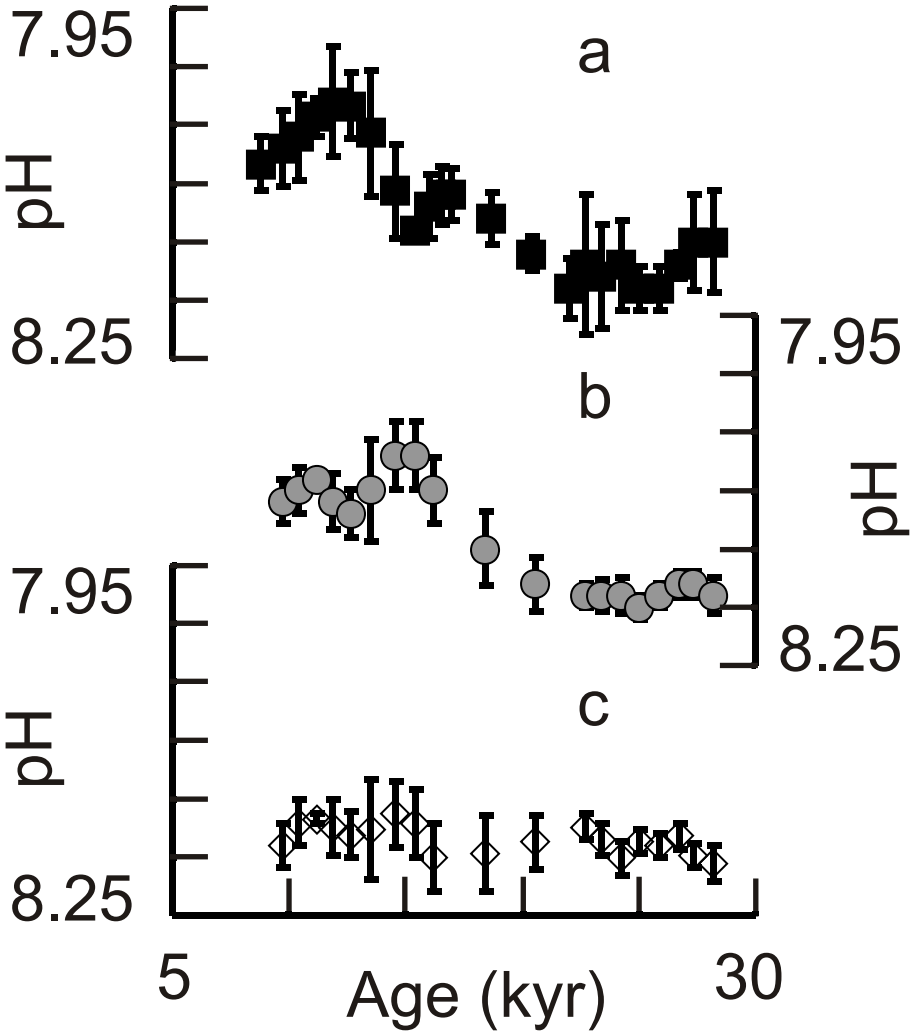

Figure 4

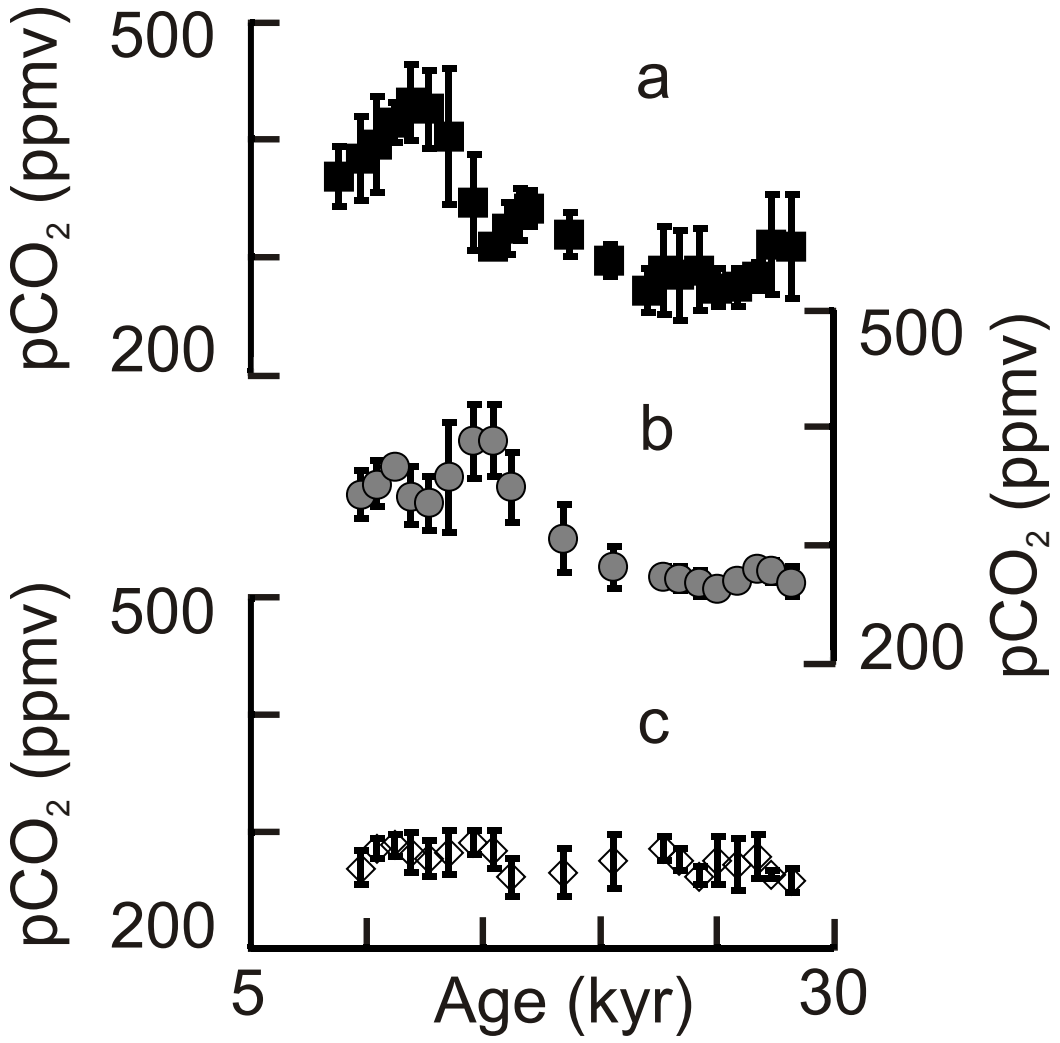

Figure 5

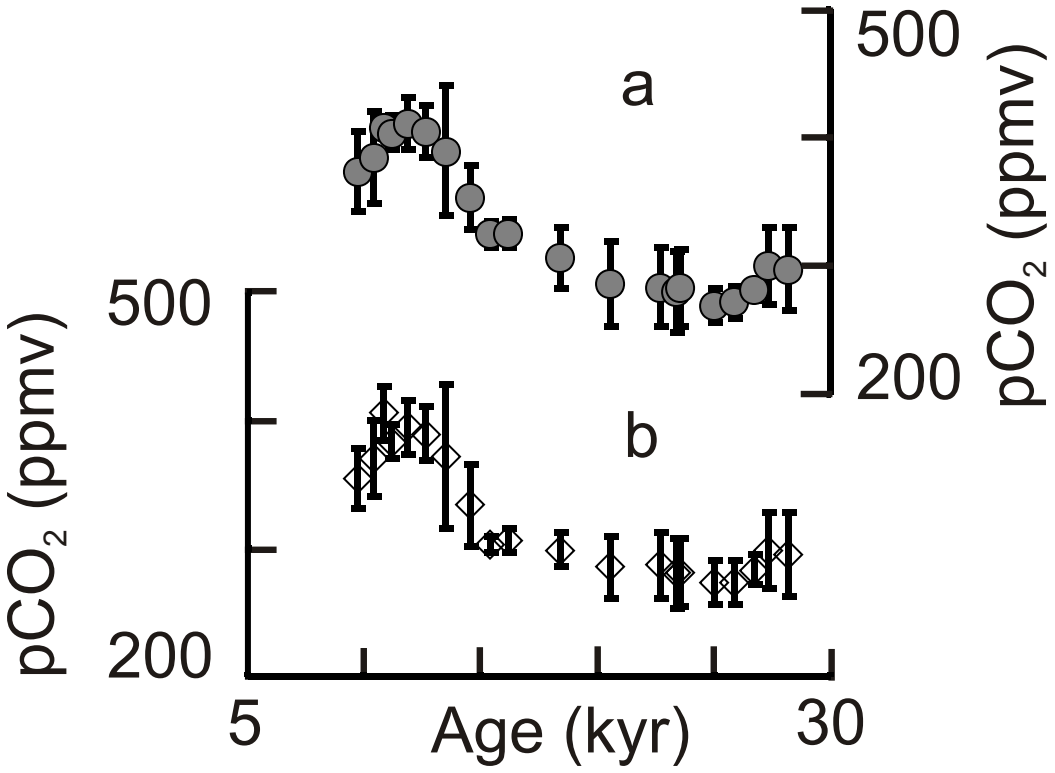

Figure 6

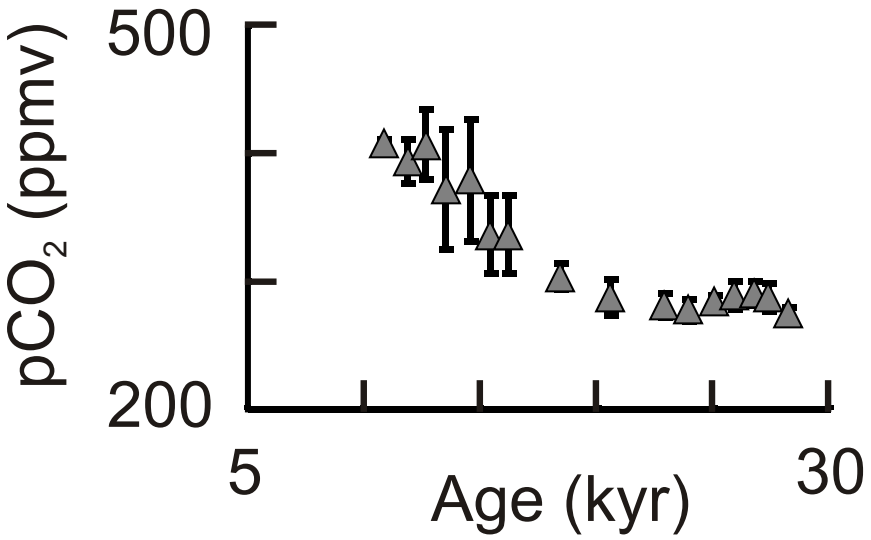

Figure 7

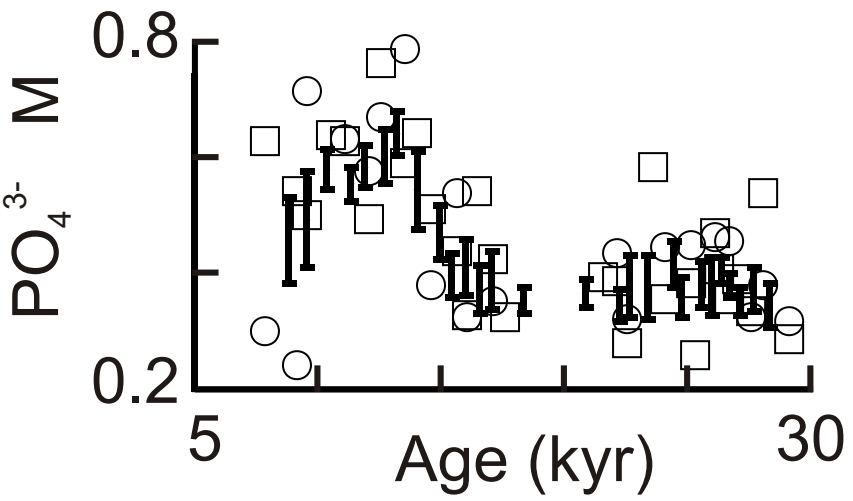

Figure 8

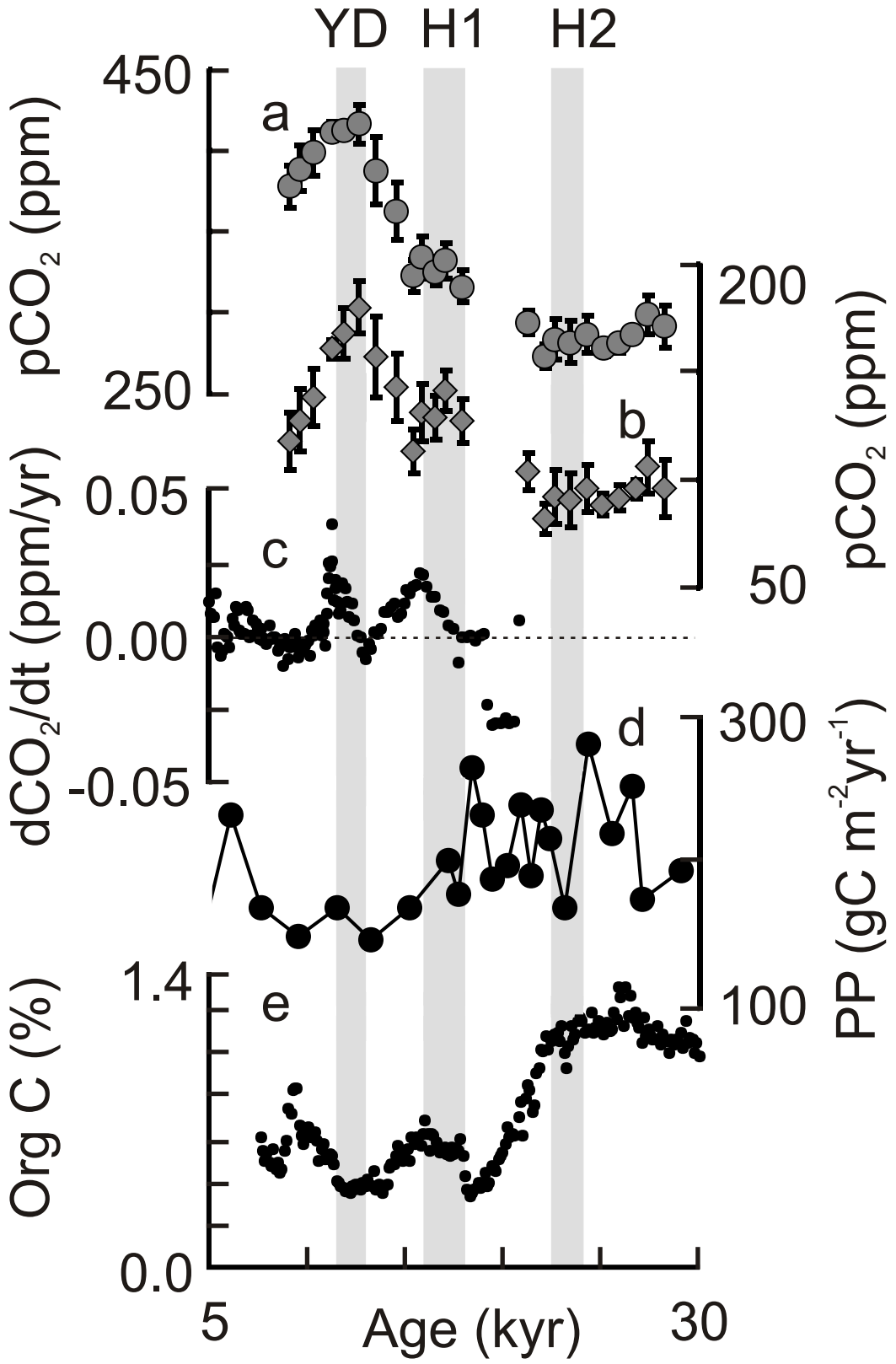
YD
H1
H2
450
250
a
pCO2 (ppm)
200
50
b
pCO2 (ppm)
0.05
0.00
-0.05
c
dCO2/dt (ppm/yr)
300
100
d
PP (gC m-2yr-1)
1.4
0.0
e
Org C (%)
5
Age (kyr)
30

Figure 9

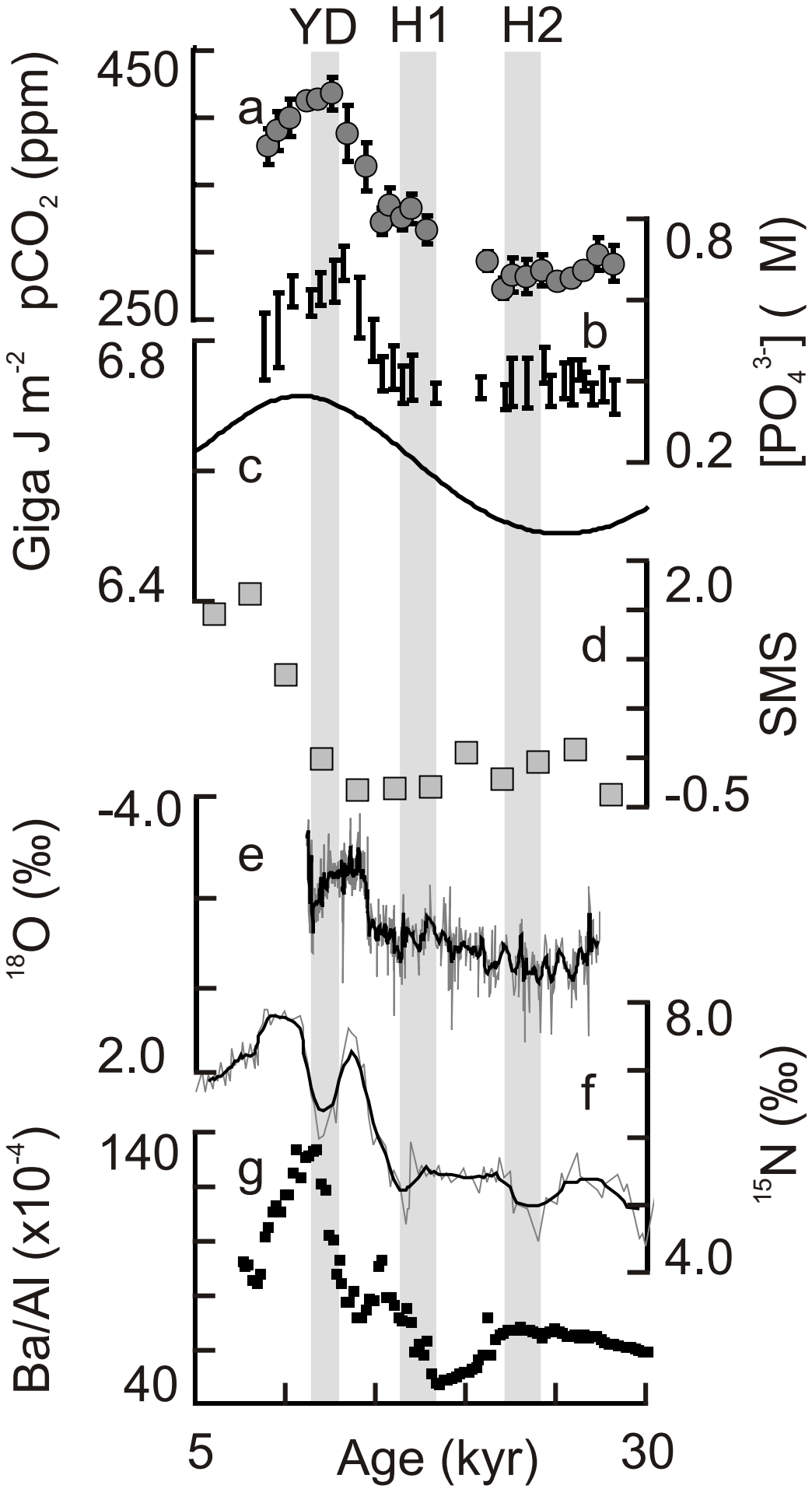
YD
H1
H2
450
250
a
pCO2 (ppm)
0.8
0.2
b
[PO4 3-] (M)
6.8
6.4
c
Giga J m-2
2.0
-0.5
d
SMS
-4.0
2.0
e
18O (‰)
8.0
4.0
f
15N (‰)
140
40
g
Ba/Al (x10-4)
5
Age (kyr)
30

Figure 10

Table 1.

			G. sacculifer			*G. ruber*	alkenone	
Sample	Age ka	$\delta^{11}B$	B/Ca μmol/mol	Mg/Ca mmol/mol	Cd/Ca μmol/mol	$\delta^{13}C$	$\delta^{13}C_{37}$	$U^{K'}_{37}$
X3	7.8	24.5		3.69		0.646	-22.55	0.972
X10	8.6					0.484	-22.87	0.926
X11	8.7					0.629	-24.05	0.931
X14	9.1	24.5	114.6	4.08	0.0184	0.661	-22.25	0.959
X18	9.5	24.9	104.0	3.71	0.0464	0.660	-22.28	0.986
X27	10.5	24.3	106.1	4.16		0.764	-23.44	0.949
X32	11.1	24.2	100.7	3.87	0.0441	0.697	-23.03	0.979
X40	12.0	24.5	100.8	3.92	0.0411	0.846	-24.17	0.955
X45	12.5	23.5	114.4	3.84	0.0460	0.842	-21.88	0.924
5b	13.5	23.6	105.1	3.89	0.0553	0.721	-22.96	0.969
9	14.0					0.804	-23.31	0.886
14b	14.5	25.2	96.0	4.19	0.0303	0.818	-22.86	0.928
23b	15.6	25.2	102.3	4.16	0.0424	0.898	-23.67	0.952
27b	16.0	25.3	109.9	4.04	0.0244	0.691	-23.49	0.966
30b	16.4	24.7				0.431	-23.72	0.904
36	17.0	24.9	118.5	4.05	0.0261	0.465	-24.04	0.892
40b	17.5	25.1				0.647	-23.74	0.949
51	18.7					0.430	-23.63	0.844
75	21.5	25.1				0.781	-22.01	0.923
80	22.1	25.3	105.0	3.29	0.0232	0.635	-22.34	0.851
84	22.5	25.7	105.1	3.35	0.0176	0.454	-22.37	0.895
93	23.6	24.7	110.4	3.62		0.219	-21.75	0.902
97	24.0	25.5	112.4	3.44	0.0255	0.280	-21.79	0.915
106	25.1	25.6	117.3	3.56	0.0273	0.727	-21.32	0.859
107	25.2					0.485	-23.13	0.888
114	26.0	25.0	100.8	3.25	0.0243	0.121	-21.50	0.902
116	26.2					0.421	-22.37	0.877
119	26.6	25.5	113.8	3.66	0.0289	0.530	-22.18	0.914
122	26.9					0.310	-22.81	0.879
127	27.5	25.3	109.8	3.64	0.0205	0.169	-22.91	0.925
131	28.0	24.4	112.5	3.50	0.0224	0.458	-21.72	0.912
140	29.0	25.5	119.6	3.58	0.0194	0.453	-22.03	0.924